# Bidirectional Single-phase Solid-State Transformer using Multi Cell for Volume Reduction of High Voltage Capacitor

Jun-ichi Itoh, Kazuki Aoyagi and Toshiki Nakanishi
Department of Electrical Engineering
Nagaoka University of Technology
Niigata, Japan
itoh@vos.nagaokaut.ac.jp

***Abstract*— This paper proposes a simple circuit configuration and a control strategy of Solid-State Transformer (SST). In the proposed circuit, it is possible to reduce the volume of heat sinks and passive components by using low voltage switching device with low loss characteristic and high frequency operation. Moreover, the circuit employed with the proposed control strategy operates stably even when the ripple voltage is large. Besides, the bidirectional operation of the proposed circuit is also confirmed by simulation. From the simulation result, the capacitance in each cell of the primary side (high voltage side) can be minimized to only 3 μF for 10-kVA system. Moreover, a miniature model with three cells is tested to confirm the fundamental operation of the proposed circuit. As a results, the sinusoidal waveform of the input current is obtained without the large distortion. the total harmonic distortion (THD) of the input current is 2.55%. In addition, it is confirmed that the primary side capacitor voltage of each cell is kept constant without the balance control.**

***Keywords—Solid-State Transformer; Power factor correction converter; LLC resonant converter; High-frequency transformer***

## I. INTRODUCTION

Recently, a smart-grid has attracted attention due to an increase of renewable energy [1]. In particular, a DC distribution system in the smart-grid has been actively researched in order to achieve the energy-saving of the data-center and the large building [2-3]. In the conventional distribution system, the AC-DC converter is required to each system, whereas in the DC distribution system, the AC-DC converter is not required. Thus, the volume of the DC distribution system is reduced [4].

Moreover, in the conventional distribution system, transformers are utilized to achieve the step-down from the grid voltage of several kilovolts to the distribution voltage of several hundred volts [5]. However, the conventional transformers are bulky and heavy because the transformers operate at the low grid frequency (50 Hz or 60 Hz).

As one of the solutions to reduce the volume and the weight of the transformer, Solid-State Transformer (SST) has been researched actively [6-8]. SST simultaneously achieves the insolation and the step-down function by using high frequency transformer. Most of all, by applying SST, it is possible to significantly reduce the system volume compared to the conventional transformer because the transformer in SST operates at the frequency of several ten-kHz. To sum up, SST has following advantages [9]:

- Reduced size and weight of system
- Power factor correction
- Harmonic suppression
- Active/ Reactive power control

In the medium voltage SST, it is possible to construct the cell converters with the multilevel topology, which contributes to the reduction of the rating voltage of the switching device. Thus, the switching devices with the low ON-state resistance and the high speed switching are applied. Moreover, the inductor volume can also be reduced [10].

However, the number of switching device is greatly increased in the multilevel topology. In particular, the control becomes complicate because the gate signal is increased with the increase of switching device [11]. Furthermore, in the conventional SST, a bulky capacitor at the DC link with a large capacitance is required in order to maintain the constant capacitor voltage in each cell [12-13]. This capacitor restricts the volume reduction.

In this paper, first of all, a simple circuit configuration of the single-phase SST is proposed. The proposed circuit can reduce the number of the switching devices compared to the conventional circuit. It contributes to the simplification of the system. Moreover, the converter volume can be reduced by applying the multi-cell topology with the small capacitors. Second, the control strategy is proposed under the condition of the large ripple voltage in each primary-side capacitor. Third, the bidirectional operations of SST under the condition of the stable state and the circuit behavior at the sudden change of the load are confirmed by simulation. Finally, the proposed SST is tested by using a miniature model with three cells and the voltage of 200 V as the input voltage.

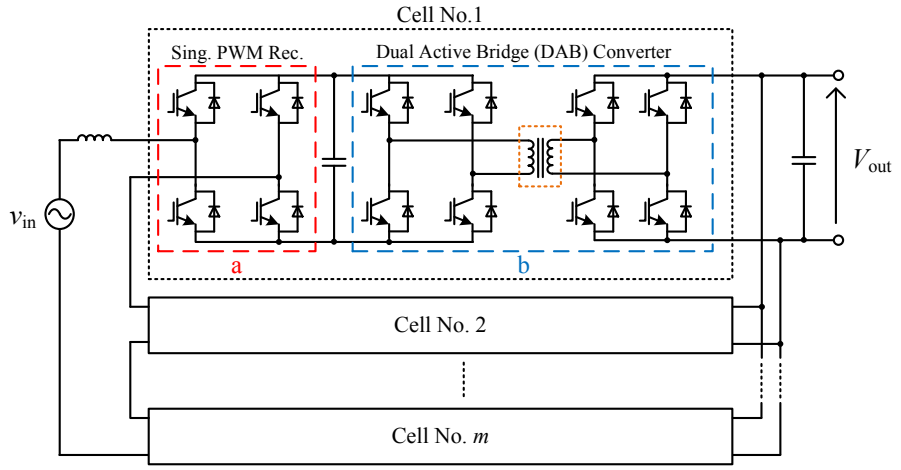


Fig. 1. Circuit configuration of conventional single-phase SST.

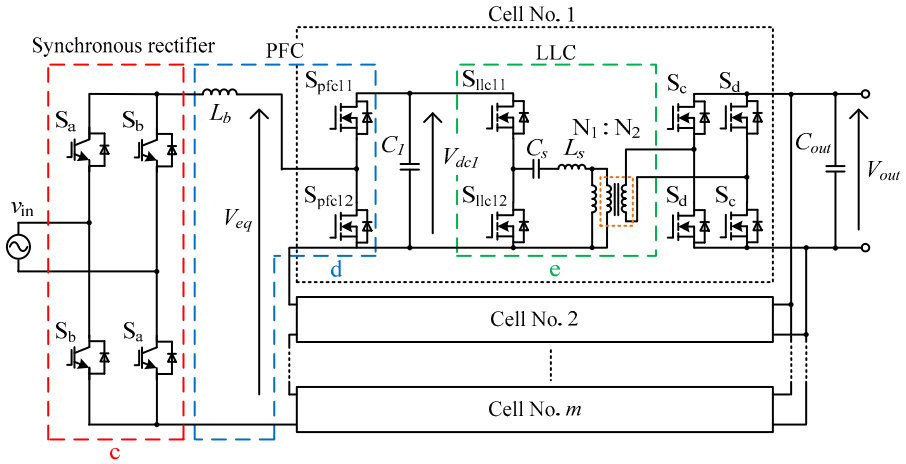


Fig.2 Circuit configuration of proposed single-phase SST.

## II. Circuit Configuration of Conventional SST and Proposed SST

Figure 1 shows the circuit configuration of the conventional single-phase SST [14-15]. The conventional SST includes the PWM rectifier and the isolated DC-DC converter with the high frequency transformer. In the conventional SST, the input side and the output side are isolated by the high frequency transformer of the dual active bridge (DAB) converter. Thus, the volume of the system is reduced because the low frequency transformer is not required. However, the number of switch increases greatly with the number of cell.

Figure 2 shows the circuit configuration of the proposed single-phase SST. In the proposed SST, the rectifier is connected to the all cell converter. Moreover, the rectifier obtains DC voltage by only switching polarity. In the rectifier, the switching device with high rating voltage are required. However, it is possible to use the switch with the slower switching speed because these switches are operated at only the low frequency (50 Hz or 60 Hz). The cell converter includes a boost converter and a half bridge LLC resonant converter as one cell. The boost converter control the input current to sinusoidal waveform with the unity power factor. In addition, the input voltage is shared equally because the grid side of the cell converter is connected in series. Thus, the voltage per cell is reduced. As a result, it is possible to use the switching of low voltage rating. In the LLC resonant converter, the volume of transformer is reduced because the transformer operates at high frequency.

Table I. Comparison of switching device between conventional SST and proposed SST.

| Number of cell | Rated Voltage | Number of Switching devices | |
|---|---|---|---|
| | | Conventional SST | Proposed SST |
| 6 | 3.3 kV | 72 | 52 |
| 11 | 1.7 kV | 132 | 92 |
| 16 | 1.2 kV | 192 | 132 |
| | | (a + b) | (c + d + e) |

Table I shows the comparison of the switch number between the conventional SST and the proposed SST. Note that the number of cell is calculated by the rated voltage of the switch. As shown in table I, the proposed SST can reduce the number of switch about 2/3 compared to that in the

conventional SST. The reason is because the proposed SST uses only one rectifier for each cell.

### A. PFC circuit (Boost converter)

The boost converter corrects the power factor of the grid side because the boost inductor current is controlled into full wave rectified waveform same as general PFC circuit. The boost inductor $L_b$ in the PFC circuit is given by (1).

$$L_b = \frac{\sqrt{2}V_{in}}{4 f_{eq} \Delta I_{Lb}} \quad \cdots\cdots(1)$$

where, $\Delta I_{Lb}$ is the ripple current of the inductor current, $f_{eq}$ is the equivalent switching frequency of the output voltage $V_{eq}$. Then, the equivalent switching frequency $f_{eq}$ is given by (2).

$$f_{eq} = m \times f_{sw} \quad \cdots\cdots(2)$$

where $m$ is the number of cell, $f_{sw}$ is the switching frequency of the PFC.

As observed in (2), the equivalent switching frequency $f_{eq}$ is proportional to the number of cell. On the other words, the equivalent frequency becomes higher by increasing the number of cells. As a result, it is possible to reduce the volume of the boost inductor $L_b$ because the ripple current decreases.

In the proposed SST, the turn ratio of transformer is designed by (3) because the operation mode always becomes the boost operation with respect of the primary side voltage.

$$N = \frac{N_1}{N_2} \geq \frac{\sqrt{2}V_{in}}{2m\lambda V_{out}} \quad \cdots\cdots(3)$$

where λ is the modulation index of the boost converter.

### B. LLC resonant converter

In the half-bridge LLC resonant converter, the zero current switching (ZCS) is achieved by using the series resonance between the leakage inductance $L_s$ of the high frequency transformer and the capacitor $C_s$ at the turn-on switching and the turn-off switching. Thus, the switching loss is greatly reduced.

Furthermore, the leakage inductance is designed to be negligibly smaller than the excitation inductance. Then, the switching frequency $f_o$ of LLC is given by (4), i.e. the resonance frequency, and the duty ratio of the switch is set to 50%.

$$f_o = \frac{1}{2\pi\sqrt{L_s C_s}} \quad \cdots\cdots(4)$$

## III. CONTROL BLOCK FOR PROPOSED SST

Figure 3 shows the control block diagram of the proposed circuit. The proposed control includes a voltage control (AVR) for the output voltage $V_{out}$ and a current control (ACR) for the boost inductor current. The balance control of the primary side capacitor voltage $V_{dc1}$ is not required, and this becomes one of the advantages of this control. In particular, when the capacitor voltage in the cell of the primary side is imbalance due to the uneven of the capacitances or the transient phenomenon of the load, the output voltage of each cell is increased or decreased according to the capacitor voltage of the primary side. Consequently, the capacitor voltage in the primary side is naturally corrected. As a result, the balance control for the high voltage capacitor is not required. Thus, the voltage management in the high-voltage side is not required. In addition, the proposed control system is simple because the AVR and the ACR are achieved by only the switches of PFC ($S_{pfc}$).

### A. Input current control and Output DC voltage control

In the input current control, the boost inductor current is controlled into full wave rectified waveform in order to correct the power factor of the grid side. Hence, the inductor current command value $I_L^*$ is given by (5).

$$I_L^* = I_{amp} \left| \sin(\omega t) \right| \quad \cdots\cdots(5)$$

where $I_{amp}$ is the output of the AVR. $I_L^*$ is generated by the multiplication of $I_{amp}$ and the full wave rectified waveform with same phase as the input voltage.

On the other hand, in the output voltage control, the output voltage is always regulated to the voltage command by using PI controller. Note that the response of the AVR is sufficiently lower than the ACR in order to avoid the interference between the AVR and the ACR. In the proposed SST, the single-phase

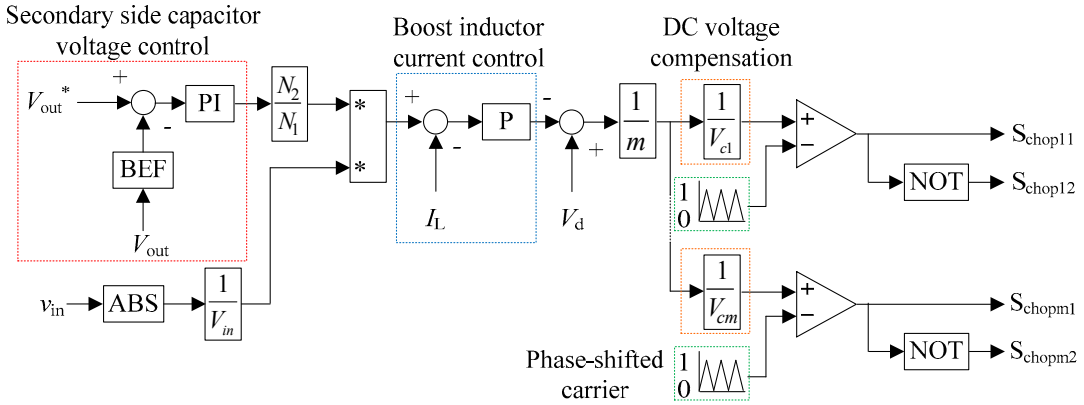


Fig. 3. Control block diagrams of proposed circuit.

Table II. Switching mode of LLC resonant converter and rectifier at power running and regeneration.

| | $S_a$, $S_b$ | $S_{llc11}$, $S_{llc12}$ | $S_c$, $S_d$ |
|---|---|---|---|
| Power running | OFF | Duty 50% switching (@50 kHz = $f_o$) | OFF |
| Regeneration | Duty 50% switching (@50 Hz) | OFF | Duty 50% switching (@50 kHz = $f_o$) |

power fluctuation occurs as a disturbance due to the use of the small-value capacitor at the primary side. As a resolution, the band elimination filter (BEF), which eliminates the voltage harmonics at 100 Hz, is applied to the voltage detection. Consequently, the AVR can control the average value of the output voltage despite the high fluctuation of the capacitor voltage at the primary side. Therefore, the design of the proposed control system becomes simple.

In the triangular wave comparator, the gate signal for PFC is generated by phase shifted carrier. Thus, the input voltage is equally divided because the switching timing is different. In addition, it is possible to use the switching device with low voltage rating. Note that the ripple current is reduced because the inductor voltage is reduced by the series connection in the PFC converter. Then, the phase shift angle $\theta$ is given by (6).

$$\theta = \frac{2k}{m}\pi \quad (k = 0, 1, \cdots, m-1) \qquad (6)$$

### B. Switching of power runnnig mode and regeneration mode

Table II shows the switching mode at the power running and the regeneration. In the power running, the switch of rectifier ($S_a$ ~ $S_d$) is always OFF, whereas the switch of LLC resonant converter ($S_{llc11}$, $S_{llc12}$) is operated. In constrast, in the regeneration, the LLC resonant converter side is always OFF, whereas rectifier side is operated.

## IV. Simulation Result

### A. Bidirectional operation of SST

Table III shows simulation conditions. The 6.6-kV grid is adopted as the input power source and the power rating of the system is 10-kVA. Then, it is assumed that the switching device with 3.3 kV voltage rating is applied to the proposed circuit.

Figure 4 shows the bidirectional operation waveforms of the proposed SST in the simulation when the primary side capacitor is 3 μF and the number of cells is six. The bidirectional operation is confirmed to in the proposed circuit. Moreover, the sinusoidal waveform of the input current is obtained without any large distortion in both operations.

In the input side, it is also confirmed that the unity power factor between the input voltage and the input current is obtained. The low input current THD of 1.71% is obtained. In the output sum voltage of each cell, it is confirmed that the waveform is seven-level staircase voltage. Furthermore, the equivalent switching frequency $f_{eq}$ is 60 kHz.

Table III. Simulation conditions.

| | | |
|---|---|---|
| Input voltage | $v_{in}$ | 6600 $V_{rms}$ |
| Rated output power | $P_{out}$ | 10 kW |
| Rated output voltage | $V_{out}$ | 320 V |
| Boost inductor | $L_b$ | 70 mH (%Z = 0.5%) |
| Primary side capacitor | $C_1$ | 3 μF |
| Resonant capacitor | $C_s$ | 0.1 μF |
| Leakage inductor | $L_s$ | 101 μH |
| Secondary side capacitor | $C_{out}$ | 3000 μF |
| Switching frequency of PFC | $f_{sw\_pfc}$ | 10 kHz |
| Resonant frequency | $f_o$ | 50 kHz |
| Number of cells | $m$ | 6 |
| Trans turns ratio | $N_1$:$N_2$ | 2.7 : 1 |

It is observed from the waveform of the capacitor voltage in the primary-side cell that, the average voltage is shared equally among all cells without the balance control and stays stably even when the ripple voltage is large. In addition, the primary side capacitor voltage includes the 10 kHz component of the switching frequency of the PFC circuit and the 50 kHz component of resonant frequency. However, it is not affect the operation because these frequency components are less than 1% against the DC component. Moreover, the capacitor voltage in the secondary side is regulated to the voltage command of 320 V. As a result, it is confirmed that the stable operation is achieved even when the primary side capacitor is small. On the other hand, the output voltage include the distortion by the single-phase power fluctuation. As a solution to reduce the distortion, the large capacitance is applied at output side.

Finally, it is observed from the waveform of the regeneration operation that the input current is reversed against the input voltage, i.e. the confirmation of the regeneration operation. The low input current THD of 1.84% is also achieved. The other waveforms are same as the waveforms of the power-running operation.

### B. Transient operation

Figure 5 shows the transient operation when the step change of the load ratio occurs in 100% to 50%, and the switching from power running to regeneration. Note that the current source is connected to the output side in order to produce the step change of the load power. The input current is decreased by 48.3% at half the load power. In addition, the input current is increased rapidly when the power running operation is switched to the regeneration operation. The reason

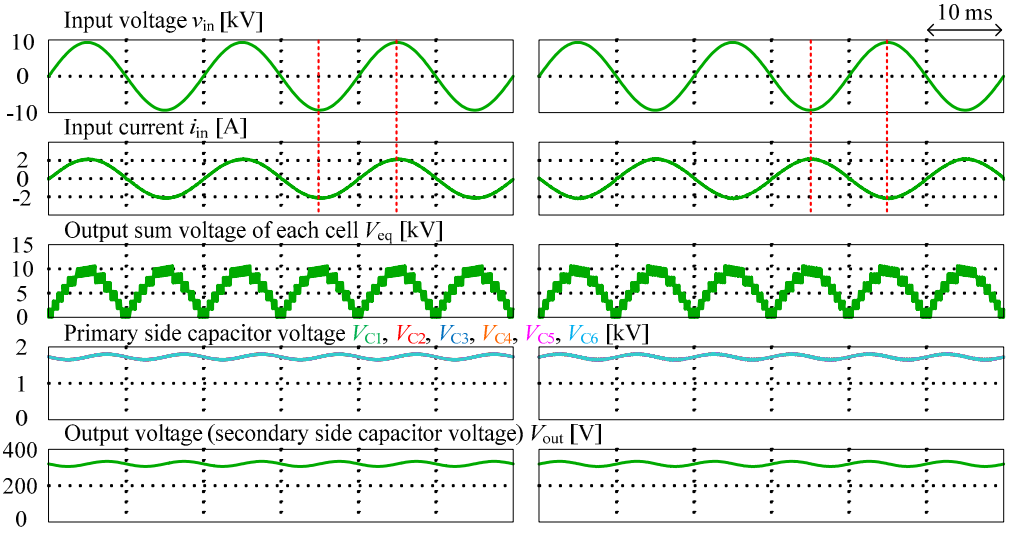


(a) Power running (b) Regeneration

Fig. 4 Operation waveform of single-phase SST.

is that the command of the power flow changes in the step response. In addition, the average voltage control of the primary side capacitor is confirmed in each cell. Moreover, the output voltage is still regulated to the voltage command of 320 V. Consequently, the stability operation of the control system is confirmed even when the load power changes suddenly.

## V. EXPRIMANTAL RESULTS

Table IV shows experimental conditions. In this experiment, the fundamental operation is verified by using a miniature model with the input voltage of 200 V when the number of cells is three. In addition, the primary side capacitor is applied the large capacitance.

Figure 6 shows the waveforms of the input voltage, the input current, the output sum voltage of each cell and the output voltage. As shown in Figure 6, the operation of the miniature model without the large distortion is confirmed.

In the input side, it is confirmed that the unity power factor between the input voltage and the input current is obtained as same as the simulation result. In particular, the input current THD of 2.55% is obtained at the rated load.

The input voltage is equally divided to each cell because the output sum voltage of each cell clearly becomes balanced multilevel waveform. Furthermore, it is also confirmed that the equivalent switching frequency $f_{eq}$ is 30 kHz. In the output side, the step-down operation is achieved because the output voltage is regulated stably to 50 V.

Figure 7 shows the primary side capacitor voltage of each cell. It is observed that the average voltage of capacitor voltage is kept constant. Moreover, the maximum value of the primary side capacitor voltage also shows same value in each cell. Thus, it is confirmed that, the primary side capacitor voltage is shared equally among all cells without the balance control.

Figure 8 shows the relationship of input current THD and output power of the SST. It is confirmed that the input current

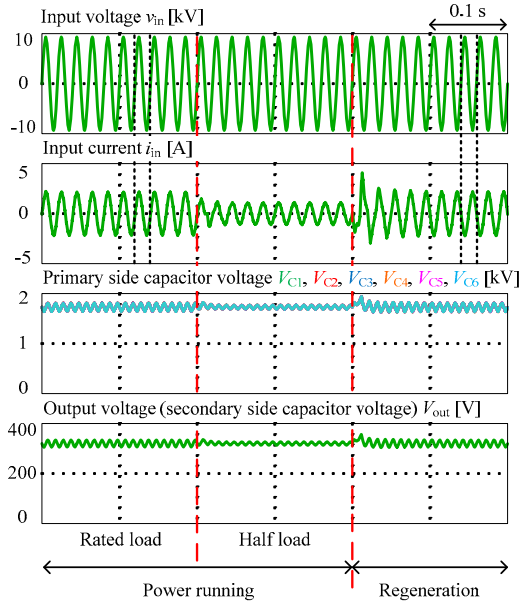


Fig. 5 Operation waveform at sudden change of load.

Table IV. Experimental conditions.

| | | |
|---|---|---|
| Input voltage | $v_{in}$ | 200 $V_{rms}$ |
| Rated output power | $P_{out}$ | 300 W |
| Rated output voltage | $V_{out}$ | 50 V |
| Boost inductor | $L_b$ | 9 mH (%Z = 2.1%) |
| Primary side capacitor | $C_1$ | 48 μF |
| Resonant capacitor | $C_s$ | 204 nF |
| Leakage inductor | $L_s$ | 50 μH |
| Secondary side capacitor | $C_{out}$ | 3300 μF |
| Switching frequency of PFC | $f_{sw\_pfc}$ | 10 kHz |
| Resonant frequency | $f_o$ | 50 kHz |
| Number of cells | $m$ | 3 |
| Trans turns ratio | $N_1$:$N_2$ | 1 : 1 |

THD becomes larger when the output power of the SST is low. The reason is that the low order harmonics component appears remarkably with respect with the fundamental component because the low input current occurs when the output power of SST is low.

## VI. CONCLUSION

This paper proposed the simple circuit configuration and the control strategy of the SST in order to reduce the system volume. The bidirectional operation of the proposed circuit was confirmed with six cells. In the capacitor voltage in the cell of the primary side, the average voltage was shared equally and stably among all cells without the voltage balance control. Moreover, the stability operation of the control system was confirmed even when the load power was suddenly changed. In the experimental result, the fundamental operation was confirmed as same as the simulation. The sinusoidal waveform of the input current was obtained without the large distortion. Moreover, it was also confirmed that the unity power factor between the input voltage and the input current was obtained. Furthermore, the average voltage of primary side capacitor was shared equally among all cells

In future, the operation with the small-value capacitor at the primary side will be confirmed by experiment.

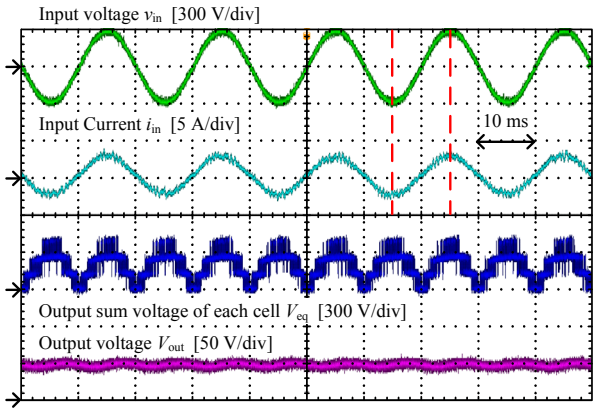


Fig. 6. Operation waveform of miniature model SST.

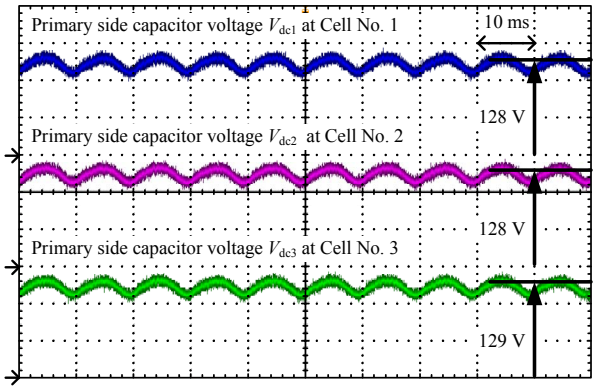


Fig. 7. Operation waveform of each primary side capacitor voltage.

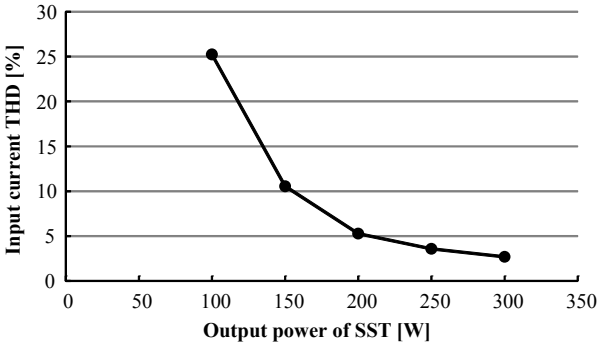


Fig. 8. Relationship of input current THD and output power of SST

## References


[1] X. She, X. Yu, F. Wang and A. Q. Huang: "Design and Demonstration of a 3.6-kV-120V/10-kVA Solid-State Transformer for Smart Grid Application" , IEEE Trans., Vol.29, No.8, pp.3982-3996 (2014)

[2] Meiqin Mao, etc. "Accurate Output Power Control of Converters for Microgrids Based on Local Measurement and Unified Control", IEEJ Journal of Industry Applications, Vol.4, No.4, pp.331-338, (2015)

[3] Ritwik Chattopadhyay, etc. "Low-Voltage PV Power Integration into Medium Voltage Grid Using High-Voltage SiC Devices", IEEJ Journal of Industry Applications, Vol.4, No.6, pp.767-775, (2015)

[4] T. Nakanishi, K. Orikawa, J. Itoh: "Modular Multilevel Converter for Wind Power Generation System Connected to Micro-Grid", ICRERA2014, No. 219, (2014)

[5] T. Nakanishi and J. Itoh: "Capacitor Volume Evaluation based on Ripple Current in Modular Multilevel Converter", 9th International Conference on Power Electronics, No.WeA1-5 (2015)

[6] Mizuki Nakahara, and Keiji Wada, "Loss Analysis of Magnetic Components for a Solid-State-Transformer", IEEJ Journal of Industry Applications, Vol.4, No.7, pp.387-394, (2015)

[7] X. Yu, X, She, X. Zhou, X. Ni and A. Q. Huang: "Sysytem Integration and Hierarchical Power Management Strategy for a Solid-State Transformer Interfaced Microgrid System", IEEE Trans., Vol.29, No.8, pp.4414-4425 (2014)

[8] X. Yu, X, She, X. Zhou and A. Q. Huang: "Power Management for DC Microgrid Enabled by Solid-State Transformer", IEEE Trans., Vol.5, No.2, pp.954-965 (2014)

[9] J. W. Kolar and G. Ortiz: "Solid-State-Transformers: Key Components of Future Traction and Smart Grid Systems", IPEC 2014, pp.22-35 (2014)

[10] Y. Noge, J. Itoh: "Linear PFC Regulator for LED Lighting with the Multi-Level Structure and Low Voltage MOSFETs", APEC2014, pp. 3311-3317 (2013)

[11] H.Hwang, X. Liu, J. Kim and H. Li: "Distributed Digital Control of Modular-Based Solid-State Transformer Using DSP+FPGA" IEEE Trans., Vol.60, No.2, pp.670-680 (2013)

[12] X. She, A. Q. Huang and R. Burgos: "Review of Solid-State Transformer Technologies and Their Application in Power Distribution Systems", IEEE Journal, Vol.1, No.3, pp.186-198 (2013)

[13] J. Shi, W. Gou, H. Yuan, T.Zhao and A. Q. Huang: "Research on Voltage and Power Balance Control for Cascaded Modular Solid-State Transformer" IEEE Trans., Vol.26, No.4, pp.1154-1166 (2011)

[14] J. Huber and J. W. Kolar: "Solid-State Transformers – On the Origins and Evolution of Key Concepts", IEEE Industrial Electronics Magazine, pp.19-28, (2016)

[15] X. She and A. Q. Huang: "Current Sensorless Power Balance Strategy for DC/DC Converters in a Cascaded Multilevel Converter Based Solid State Transformer" IEEE Trans., Vol.29, No.1, pp.17-22 (2014)